Topological Creation and Destruction of Edge States in Photonic Graphene

Mikael C. Rechtsman,[1,*] Yonatan Plotnik,[1] Julia M. Zeuner,[2] Daohong Song,[3] Zhigang Chen,[3,4]
Alexander Szameit,[2] and Mordechai Segev[1]

[1]*Physics Department and Solid State Institute, Technion, Haifa 32000, Israel*
[2]*Institute of Applied Physics, Abbe Center of Photonics, Friedrich-Schiller-Universität Jena, Max-Wien-Platz 1, 07743 Jena, Germany*
[3]*The Key Laboratory of Weak-Light Nonlinear Photonics, Ministry of Education and TEDA Applied Physics School,*
Nankai University, Tianjin 300457, China
[4]*Department of Physics and Astronomy, San Francisco State University, San Francisco, California 94132, USA*

We experimentally demonstrate a topological transition of classical light in "photonic graphene": an array of waveguides arranged in the honeycomb geometry. As the system is uniaxially strained (compressed), the two unique Dirac points (present in the spectrum of conventional graphene) merge and annihilate each other, and a band gap forms. As a result, edge states are created on the zigzag edge and destroyed on the bearded edge. These results are applicable for any 2D honeycomb-type structure, from carbon-based graphene to photonic lattices and crystals.

The rise of the first truly two-dimensional material, graphene, started with its discovery in 2004 [1] and has continued as a result of its potential in electronic and optoelectronic devices, including applications in flexible electronics [2], optical modulation [3], and metamaterials [4]. Graphene is also extremely important in the fundamental understanding of condensed matter [5]. The reason is the presence of two unique Dirac cones in graphene's band structure, leading to dynamics governed by the Dirac equation, instead of the more typical Schrödinger equation; this causes electrons to propagate like massless relativistic fermions. Indeed, a model of a graphenelike structure was used in proposing the first topological insulator [6–8], a material with conducting edges whose propagating edge states are immune to disorder. This immunity has led to active research into whether such edge states can remain entangled for long times, and act as robust qubits in a quantum computer [8]. The striking feature of topological physical properties is that they are not affected by small perturbations (at any order in perturbation theory). For example, edge states of two-dimensional topological insulators cannot backscatter unless the scattering potential breaks time-reversal symmetry or is large enough to close the bulk gap. Graphene, while not a topological insulator, possesses edge states that are "topologically protected" only in the sense that their presence is derived from a topological property (the Berry phase) and cannot be destroyed by weak perturbations that respect certain symmetries [9–11] (this should not be confused with topological protection against backscattering [7]). Indeed, in the tight-binding limit, perturbations that respect the chiral symmetry of the structure (for example off-diagonal disorder) do not perturb the edge state energies [12,13]. Only for very strong perturbations can a "topological transition" be observed: the Dirac points merge and a bulk band gap is opened [14].

The dispersion properties of graphene have been exploited in the field of photonics as well. Photonic Dirac cones have been demonstrated experimentally [15] and studied theoretically [15–23]. Experiments have addressed conical diffraction [15], topological protection of edge states in magnetically active photonic crystals [24], enabling single photonic mode behavior over large areas [25], pseudomagnetic behavior at optical frequencies [26], and finally—the first experimental realization of an external-field-free photonic topological insulator [27]. Systems exhibiting photonic Dirac cones include photonic lattices (waveguide arrays) [15,19,20,22], and two- and three-dimensional photonic crystals [25,28]. Edge states that can be derived from topological arguments have also been theoretically predicted [29,30] and demonstrated optically in systems without Dirac cones, namely, photonic quantum walks [31], one-dimensional dimer waveguide arrays [32], and one-dimensional quasicrystalline waveguide arrays [33]. Light propagating in photonic lattices with honeycomb geometries obeys the same equation as electrons in graphene, namely, the Schrödinger equation with a honeycomb potential. Therefore, such a "photonic graphene" lattice emulates carbon-based graphene just as Bose-Einstein condensates in optical lattices emulate condensed matter phenomena. Indeed, many of the topological properties of graphene carry over to photonics.

In this Letter, we present theoretically and experimentally a topological transition in photonic graphene. A photonic graphene lattice is compressed (or uniaxially strained) and undergoes a transition—as a function of the degree of compression—from an ungapped phase with two unique Dirac points, to a phase where the Dirac points have merged and a band gap opens [11,18]. This transition is universal to any honeycomb-shaped potential in any wave system, yet the compression required in observing

this transition is beyond the applicable strain levels in carbon-based graphene. Indeed, the presence of such Dirac cones and their motion in the Brillouin zone is purely a result of the honeycomb symmetry, as evidenced by numerous other wave systems in which this graphenelike behavior has been observed. These include of course graphene itself [1], two-dimensional photonic crystals [28,34] (which are in the extreme nonparaxial limit), ultracold fermionic systems [35], and molecular crystals [36]. Hence, photonic graphene provides an ideal setting for experimenting with this phenomenon. Since each of the Dirac points in the uncompressed graphene has a Berry phase of π and $-\pi$, respectively, they are topologically protected against small strains or compressions that preserve inversion symmetry (which the compression indeed preserves). We experimentally demonstrate that when the compression reaches a certain critical threshold, the states localized on the edges undergo a transition. Namely, the edge states associated with the so-called "bearded" (or "Klein") edge disappear when the Dirac points merge, while conversely, the edge states associated with the "zigzag" edge then occupy the entire edge Brillouin zone. This behavior is associated with the merging of the Dirac points and the subsequent formation of a bulk band gap, as was shown theoretically in Ref. [11]. Microscope images of the input facets of the photonic lattices are shown in Fig. 1(a), and the edge terminations are labeled.

The paraxial discrete Schrödinger equation describes the diffraction of light through a photonic lattice [37,38]:

$$ i\partial_z \psi_n(z) = \sum_{\langle m \rangle} c(|\boldsymbol{r}_{n,m}|) \psi_m(z) \equiv H_{m,n} \psi_m. \quad (1) $$

Here, z is the distance of propagation; ψ_n is the amplitude of the guided mode in the nth waveguide; $c(|\boldsymbol{r}_{m,n}|)$ is the coupling constant between waveguides m and n when they are placed a distance $|\boldsymbol{r}_{m,n}|$ apart from one another; H is the Hamiltonian matrix; and the summation is taken over only the nearest neighbor waveguides. The validity of this equation for describing the system used in this Letter has been established previously [38,39]. Note that this equation is equivalent to a tight-binding model of electrons in a lattice, where the z coordinate takes the place of the time coordinate of electron evolution. Thus as light diffracts through the lattice, it behaves analogously to electrons evolving in time in the solid state.

The waveguide array is arranged in a honeycomb lattice, as shown in Fig. 1(a). We fabricate six samples, with an increasing degree of compression in the vertical direction [Fig. 1(b) shows the sample with the greatest compression]. The vertical coupling constant, c_1, increases more rapidly with compression than the diagonal coupling constant, c_2 [see inset of Fig. 1(a)]. While the waveguides have an elliptic shape, this has little effect on the results. In the honeycomb lattice, the Hamiltonian may be represented as $H(\boldsymbol{k}) = \boldsymbol{h}(\boldsymbol{k}) \cdot \boldsymbol{\sigma}$, where

$$ \boldsymbol{h}(k) = \left(c_1 + 2c_2 \cos\left(\frac{k_x}{2}\right)\cos\left(\frac{\sqrt{3}k_y}{2}\right), 2c_2 \cos\left(\frac{k_x}{2}\right) \right. $$
$$ \left. \times \sin\left(\frac{\sqrt{3}k_y}{2}\right) \right), \quad (2) $$

where $H(\boldsymbol{k})$ is the Hamiltonian represented in lattice momentum $[\boldsymbol{k} = (k_x, k_y)]$ space and $\boldsymbol{\sigma} = (\sigma_x, \sigma_y)$ is a two-dimensional vector of the x and y Pauli matrices. Diagonalization results in the band structure diagrams shown in Figs. 2(a) and 2(b), for the cases of the uncompressed honeycomb lattice ($c_1 = c_2$) and the highly compressed lattice ($c_1 = 2.5c_2$). Note that the meaning of the eigenvalue of the Hamiltonian is the wave number in the z direction (also known as the propagation constant), or $\beta(\boldsymbol{k})$. In the uncompressed case, the band structure exhibits Dirac cones (conical intersections of the two bands), two of which are inequivalent (all others are separated by a reciprocal lattice vector from the principal two). When the
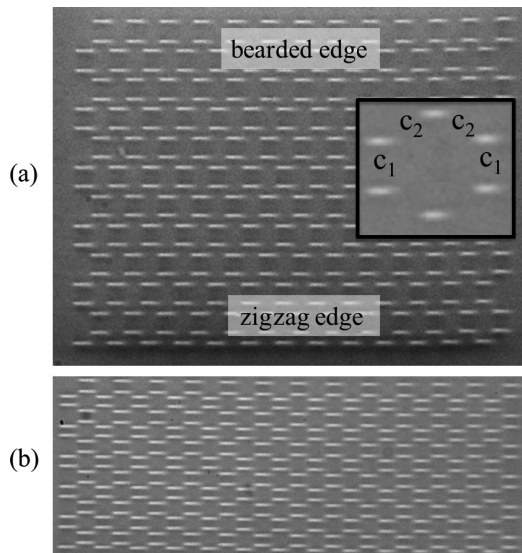

(a)

(b)

FIG. 1. Microscope images of the input facets of the uncompressed, $s = 1.0$ (a) and strongly compressed, $s = 0.5$ (b) honeycomb waveguide array. Inset to (a) shows the vertical coupling constant c_1 and diagonal coupling constant c_2.
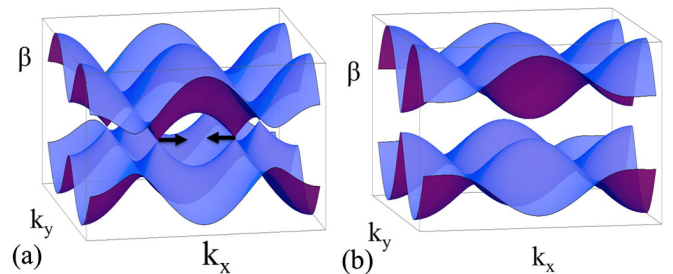

FIG. 2 (color online). Spatial band structure of the (a) uncompressed and (b) compressed honeycomb photonic lattice. The black arrows in (a) indicate the direction that the Dirac points move when the system is compressed.

lattice is compressed, the Dirac cones approach each other [as indicated by the black arrows in Fig. 2(a)] [14,20]. When the compression is such that $c_1 = 2c_2$, the cones merge, and a band gap is opened for $c_1 > 2c_2$ [20].

The presence of edge states can be analytically derived from the "bulk-edge correspondence" [10,11,40–42] via a calculation involving the Berry phase (or "Zak phase [43]")—a topological property of the band structure. The Berry phase is

$$\gamma = i \oint d\mathbf{k} \cdot \langle \phi_{\mathbf{k}} | \nabla_{\mathbf{k}} | \phi_{\mathbf{k}} \rangle, \qquad (3)$$

where the integral is over a closed loop in $\mathbf{k}$ space, and $|\phi_{\mathbf{k}}\rangle$ is an eigenstate of the Hamiltonian at Bloch wave vector $\mathbf{k}$. The eigenstate can be expressed as $|\phi_{\mathbf{k}}\rangle = (1, e^{i\theta_k})/\sqrt{2}$, where θ_k is a real phase that is a function of $\mathbf{k}$. It can be shown [43] that γ is a *topological invariant* of a lattice system—i.e., that small changes in the nature of the shape of the loop cannot change the value of γ. Moreover, specifically in the honeycomb lattice $\gamma = w\pi$, w being the *winding number* of the vector field $\mathbf{h}(\mathbf{k})$. Note that the angle that $\mathbf{h}(\mathbf{k})$ makes with the positive h_x axis is exactly θ_k, and Eq. (3) amounts to integrating $\theta_k/2$ along the given integration path. Thus, if along the path through $\mathbf{k}$ space the vector $\mathbf{h}(\mathbf{k})$ makes a complete loop, then $\gamma = \pm\pi$, otherwise, $\gamma = 0$. Furthermore, small compressions of the lattice do not change these values. In Fig. 3(a), we represent this calculation pictorially, with the Dirac points indicated by black dots. The path taken by the integral follows the green and red vertical lines, and the arrows represent the direction of the vector $\mathbf{h}(\mathbf{k})$. Even though the integration paths are vertical, they are in fact closed loops because the Brillouin zone is periodic, and thus the path effectively closes. The diagram is shown for the bearded edge termination, when it is repeated in the x direction but is terminated in the y direction. The bulk-edge

correspondence theorem states that if $\gamma = \pi$, there will be an edge state at the value of k_x corresponding to the vertical line, whereas if $\gamma = 0$, there will not. It is clear from the arrows in Fig. 3(a) that, in the shaded region, the vector $\mathbf{h}(\mathbf{k})$ makes a complete loop and thus there are bearded edge states at these values of k_x, whereas in the unshaded regions there are not. The zigzag edge contains states for values of k_x for which the bearded edge contains none (unshaded regions), and does not contain edge states for which the bearded edge does (shaded regions).

As the lattice is compressed, the Dirac points get closer to one another in pairs, then merge and open a band gap when $c_1 = 2c_2$ [20]. Until they merge, they are topologically protected against opening a band gap due to the Berry phase associated with circular loops around them (see Supplemental Material [44] Sec. 1 for more details on the nature of the topological protection of the Dirac points). Figure 3(b) shows an equivalent plot to that of Fig. 3(a), but for supercritical compression ($c_1 = 2.5c_2$). Here, the Dirac points have merged, eliminating the bearded edge state [i.e., the shaded region of Fig. 3(a)]. Conversely, the zigzag edge then occupies the entire edge Brillouin zone (i.e., all values of k_x). The diagram equivalent to Fig. 3, but for the zigzag edge, is shown in Sec. 2 of the Supplemental Material [44]. To confirm the presence (and absence) of the edge states on the bearded and zigzag edges, we compute the edge band structures for a number of different values of the compression, s. This is done by choosing a unit cell that is periodic in the x direction, but which is terminated with either the bearded or zigzag edges in the y direction. The result of this calculation (which uses the full Schrödinger equation with laboratory parameters) is discussed in Sec. 3 of the Supplemental Material [44].

In our experiments, the honeycomb waveguide array is written using the femtosecond-direct-laser-writing technique [39], in fused silica. The waveguides are elliptical in shape, with horizontal and vertical diameters of 11 and 3 μm, respectively. The index of refraction of the ambient silica is 1.45, and the change of index associated with the waveguides is 6×10^{-4}. The spacing between waveguides is 22 μm, making the lattice constant $a = 22 \times \sqrt{3}$ μm. To probe where the edge state resides as a function of k_x, we perform "spatial spectroscopy" on the edge. An elliptical beam of light (at wavelength 633 nm, from a helium-neon laser) is launched at the input facet, such that it is localized at the edge, but is broad in the direction parallel to the edge. The broadness of the beam in the x direction implies that it is narrow in k_x space and thus excites states in a narrow line width around k_x. The elliptical beam is tilted horizontally in order to tune the value of k_x, thus applying a linear phase gradient in the x direction. The precise details of the experimental setup are described in detail in Ref. [45].

Next, we present the numerical and experimental results associated with edge confinement, starting first with the bearded edge [the top of the waveguide array depicted in
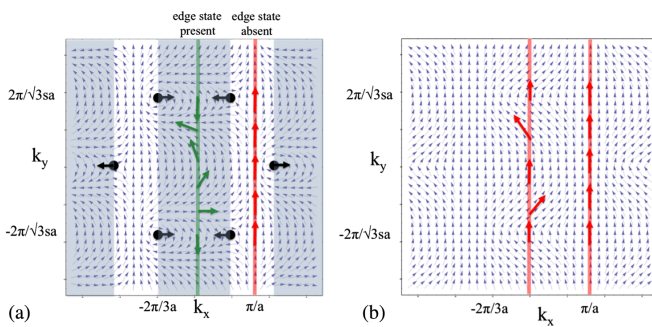

edge state present   edge state absent

(a) $-2\pi/3a$ k_x π/a (b) $-2\pi/3a$ k_x π/a

FIG. 3 (color online). Schematic of Berry's phase calculation demonstrating the values of k_x for which a bearded edge state exists, via the bulk-edge correspondence theorem, for both (a) the uncompressed ($s = 1$), and (b) strongly compressed ($s = 0.5$) cases. The arrows point in the direction of the vector $\mathbf{h}(\mathbf{k})$. In (a), the black dots indicate the Dirac points, and the arrows indicate the direction they move upon compression. Bearded edge states are present in the shaded regions of (a), and are not present in (b).
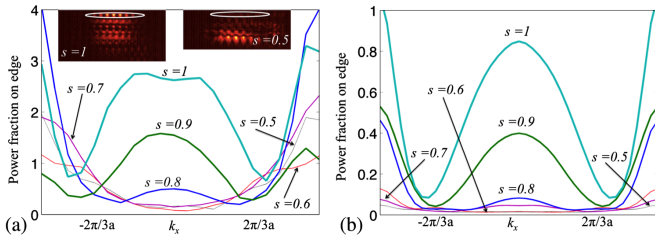
FIG. 4 (color online).   Ratio of optical power on the bearded edge to that diffracted into the bulk, as a function of k_x: (a) shows experimental results, and (b) shows numerical results from beam-propagation simulations. Top left and right insets in (a) show the output beam at $k_x = 0$ when $s = 1$ and 0.5, respectively. The white ellipse indicates the position of the input beam on the bearded edge.

FIG. 5 (color online).   Similar to Fig. 4, but for the zigzag edge.

Fig. 1(a)]. The numerical results are obtained using the beam propagation method, in which the continuous Schrödinger equation is evolved in "time" (in propagation distance, z) in a finite honeycomb array. Figures 4(a) and 4(b) show (experiment and simulation, respectively) the ratio of optical power remaining on the edge at the output facet (within the first two rows of waveguides) relative to the power diffracted into the bulk, plotted as a function of Bloch wave number, k_x, within the edge Brillouin zone. Indeed, simply by tuning the incident angle of the input beam, we can directly probe the presence or absence of an edge state as a function of Bloch momentum. Here, we let s denote the degree of compression in the vertical direction: if the height of the perfect honeycomb lattice is h, then the height of the compressed lattice is sh. Results are presented for arrays compressed in the vertical direction by a factor of $s = 0.5$, 0.6, 0.7, 0.8, 0.9, and 1.0, yielding coupling constant ratios of $c_1/c_2 = 3.6$, 2.6, 1.9, 1.5, 1.1, and 0.9, respectively. Note that the ratio of the vertical coupling, c_1, to the diagonal coupling, c_2, is at its greatest when the lattice is at its most compressed ($s = 0.5$). For $s = 1.0$, there is strong confinement surrounding $k_x = 0$, indicating an edge state. This is the edge state derived in the discussion surrounding Fig. 3. The strong edge confinement near $k_x = \pi/a$ is due to the presence of another, nontopological edge state that has been presented elsewhere [45]. The results in Fig. 4 show that with increasing compression, there is lower power on the edge, as well as a narrower region in k_x space for which power is confined. This corresponds directly to the destruction of the bearded edge state demonstrated in Fig. 3. The fraction of power remaining on the edge also decreases as a result of the further penetration of the edge states into the bulk with increasing compression. In the top left and top right insets of Fig. 4(a) we show the output facet for $k_x = 0$ and $s = 1$ (where there is an edge state), and $k_x = 0$ and $s = 0.5$ (where there is none), respectively. The white ellipse indicates the position of the input beam. In the former, light is confined to the edge due to the presence of the edge state, and in the latter case it diffracts into the bulk due to the lack thereof. Thus, we observe the destruction of the bearded edge state as a result of the merging of the Dirac points.
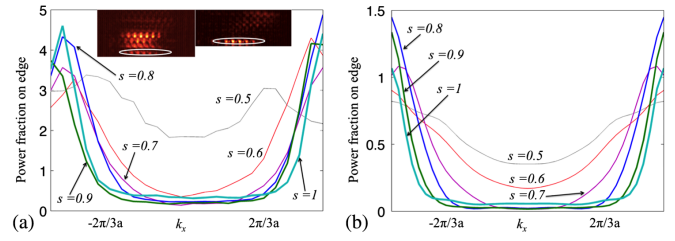
Numerical and experimental results for the zigzag edge are shown in Figs. 5(a) and 5(b), respectively. This figure is the equivalent of Fig. 4, but for the zigzag edge. Recall that the zigzag edge exhibits edge states at exactly those values of k_x for which the bearded does not. As the system is compressed, zigzag edge states thus occupy all values of k_x. The diagram showing the existence of a zigzag edge state is shown in the Supplemental Material [44]. Thus, just as the edge state was destroyed on the bearded edge, it is created on the zigzag edge. Light emerging from the output facets of the waveguide arrays are shown in the top left and top right insets of Fig. 5(a) for $k_x = 0$ with $s = 1$ (where there is no edge state), and $s = 0.5$ (where there is an edge state), respectively. Clearly, no edge confinement is observed in the former case, and strong edge confinement is observed in the latter.

In summary, we have demonstrated the destruction of graphenelike edge states on the bearded edge of a honeycomb photonic lattice, together with the simultaneous creation of edge states on the zigzag edge. This result derives from a topological mechanism in which Dirac points merge and annihilate one another as a result of compression. Topological systems are heralded for being impervious to small perturbations; this result is a prime example of how a large perturbation can tune between one topological phase and another. For example, topological transitions of the type presented would most probably occur also in Kagome lattices, which are constructed from a three-member basis.

*mcr@technion.ac.il
[1] K. S. Novoselov, A. K. Geim, S. V. Morozov, D. Jiang, M. I. Katsnelson, I. V. Grigorieva, S. V. Dubonos, and A. A. Firsov, Nature (London) **438**, 197 (2005).

[2] G. Eda, G. Fanchini, and M. Chhowalla, Nat. Nanotechnol. **3**, 270 (2008).

[3] M. Liu, X. Yin, E. Ulin-Avila, B. Geng, T. Zentgraf, L. Ju, F. Wang, and X. Zhang, Nature (London) **474**, 64 (2011).

[4] A. Vakil and N. Engheta, Science **332**, 1291 (2011).

[5] Y. Zhang, Y.-W. Tan, H. L. Stormer, and P. Kim, Nature (London) **438**, 201 (2005).

[6] C. L. Kane and E. J. Mele, Phys. Rev. Lett. **78**, 1932 (1997).

[7] M. Z. Hasan and C. L. Kane, Rev. Mod. Phys. **82**, 3045 (2010).

[8] J. E. Moore, Nature (London) **464**, 194 (2010).

[9] M. Kohmoto and Y. Hasegawa, Phys. Rev. B **76**, 205402 (2007).

[10] R. S. K. Mong and V. Shivamoggi, Phys. Rev. B **83**, 125109 (2011).

[11] P. Delplace, D. Ullmo, and G. Montambaux, Phys. Rev. B **84**, 195452 (2011).

[12] M. Wimmer, A. R. Akhmerov, and F. Guinea, Phys. Rev. B **82**, 045409 (2010).

[13] J. M. Zeuner, M. C. Rechtsman, S. Nolte, and A. Szameit, arXiv:1304.6911.

[14] G. Montambaux, F. Piéchon, J.-N. Fuchs, and M. O. Goerbig, Phys. Rev. B **80**, 153412 (2009).

[15] O. Peleg, G. Bartal, B. Freedman, O. Manela, M. Segev, and D. N. Christodoulides, Phys. Rev. Lett. **98**, 103901 (2007).

[16] R. A. Sepkhanov, Y. B. Bazaliy, and C. W. J. Beenakker, Phys. Rev. A **75**, 063813 (2007).

[17] F. D. M. Haldane and S. Raghu, Phys. Rev. Lett. **100**, 013904 (2008).

[18] O. Bahat-Treidel, O. Peleg, and M. Segev, Opt. Lett. **33**, 2251 (2008).

[19] M. J. Ablowitz, S. D. Nixon, and Y. Zhu, Phys. Rev. A **79**, 053830 (2009).

[20] O. Bahat-Treidel, O. Peleg, M. Grobman, N. Shapira, M. Segev, and T. Pereg-Barnea, Phys. Rev. Lett. **104**, 063901 (2010).

[21] O. Bahat-Treidel and M. Segev, Phys. Rev. A **84**, 021802 (2011).

[22] A. Szameit, M. C. Rechtsman, O. Bahat-Treidel, and M. Segev, Phys. Rev. A **84**, 021806 (2011).

[23] C. L. Fefferman and M. I. Weinstein, J. Am. Math. Soc. **25**, 1169 (2012).

[24] Z. Wang, Y. Chong, J. D. Joannopoulos, and M. Soljacic, Nature (London) **461**, 772 (2009).

[25] J. Bravo-Abad, J. D. Joannopoulos, and M. Soljačić, Proc. Natl. Acad. Sci. U.S.A. **109**, 9761 (2012).

[26] M. C. Rechtsman, J. M. Zeuner, A. Tünnermann, S. Nolte, M. Segev, and A. Szameit, Nat. Photonics **7**, 153 (2013).

[27] M. C. Rechtsman, J. M. Zeuner, Y. Plotnik, Y. Lumer, D. Podolsky, F. Dreisow, S. Nolte, M. Segev, and A. Szameit, Nature (London) **496**, 196 (2013).

[28] T. Ochiai and M. Onoda, Phys. Rev. B **80**, 155103 (2009).

[29] W. P. Su, J. R. Schrieffer, and A. J. Heeger, Phys. Rev. Lett. **42**, 1698 (1979).

[30] H. Schomerus, Opt. Lett. **38**, 1912 (2013).

[31] T. Kitagawa, M. A. Broome, A. Fedrizzi, M. S. Rudner, E. Berg, I. Kassal, A. Aspuru-Guzik, E. Demler, and A. G. White, Nat. Commun. **3**, 882 (2012).

[32] N. Malkova, I. Hromada, X. Wang, G. Bryant, and Z. Chen, Opt. Lett. **34**, 1633 (2009).

[33] Y. E. Kraus, Y. Lahini, Z. Ringel, M. Verbin, and O. Zilberberg, Phys. Rev. Lett. **109**, 106402 (2012).

[34] D. Jukić, H. Buljan, D.-H. Lee, J. D. Joannopoulos, and M. Soljačić, Opt. Lett. **37**, 5262 (2012).

[35] L. Tarruell, D. Greif, T. Uehlinger, G. Jotzu, and T. Esslinger, Nature (London) **483**, 302 (2012).

[36] K. K. Gomes, W. Mar, W. Ko, F. Guinea, and H. C. Manoharan, Nature (London) **483**, 306 (2012).

[37] D. N. Christodoulides and R. I. Joseph, Opt. Lett. **13**, 794 (1988).

[38] F. Lederer, G. I. Stegeman, D. N. Christodoulides, G. Assanto, M. Segev, and Y. Silberberg, Phys. Rep. **463**, 1 (2008).

[39] A. Szameit and S. Nolte, J. Phys. B **43**, 163001 (2010).

[40] S. Ryu and Y. Hatsugai, Physica (Amsterdam) **22E**, 679 (2004).

[41] Y. Hatsugai, T. Fukui, and H. Aoki, Eur. Phys. J. Spec. Top. **148**, 133 (2007).

[42] Y. Hatsugai, Solid State Commun. **149**, 1061 (2009).

[43] J. Zak, Phys. Rev. Lett. **62**, 2747 (1989).

[44] See Supplemental Material at http://link.aps.org/supplemental/10.1103/PhysRevLett.111.103901 for a more detailed discussion.

[45] M. C. Rechtsman, Y. Plotnik, D. Song, M. Heinrich, J. M. Zeuner, S. Nolte, N. Malkova, J. Xu, A. Szameit, Z. Chen, and M. Segev, arXiv:1210.5361.